MULTISCALE MODEL. SIMUL.
Vol. 4, No. 3, pp. 915–935

EQUATION-FREE, MULTISCALE COMPUTATION FOR UNSTEADY RANDOM DIFFUSION*

DONGBIN XIU† AND IOANNIS G. KEVREKIDIS‡

Abstract. We present an "equation-free" multiscale approach to the simulation of unsteady diffusion in a random medium. The diffusivity of the medium is modeled as a random field with short correlation length, and the governing equations are cast in the form of stochastic differential equations. A detailed fine-scale computation of such a problem requires discretization and solution of a large system of equations and can be prohibitively time consuming. To circumvent this difficulty, we propose an equation-free approach, where the fine-scale computation is conducted only for a (small) fraction of the overall time. The evolution of a set of appropriately defined coarse-grained variables (observables) is evaluated during the fine-scale computation, and "projective integration" is used to accelerate the integration. The choice of these coarse variables is an important part of the approach: they are the coefficients of pointwise polynomial expansions of the random solutions. Such a choice of coarse variables allows us to reconstruct representative ensembles of fine-scale solutions with "correct" correlation structures, which is a key to algorithm efficiency. Numerical examples demonstrating accuracy and efficiency of the approach are presented.

Key words. multiscale problem, diffusion in random media, stochastic modeling, equation-free

AMS subject classifications. 60H15, 60H35, 65C20, 65C30

DOI. 10.1137/040615006

1. Introduction.

This paper is devoted to numerical simulations of diffusion in a random medium whose material property, i.e., diffusivity (permeability, conductivity), is characterized by small-scale, rough structures. This problem arises in the study of composite material properties, flow in porous media, etc. (see, e.g., [5, 31]). Direct, fully resolved computations of the governing equations in such media can be prohibitively time consuming, as the fine-scale structures require discretizations resulting in large degree of freedom calculations. Hence, there has been a growing interest in designing efficient alternative methods to solve the problems with the desired accuracy.

The properties of such media are typically modeled as *deterministic* smooth functions superimposed with fast oscillatory components. One of the traditional approaches is to derive the *effective* properties of such (heterogeneous) media—the so-called homogenization or upscaling techniques. These techniques are typically based on analytical asymptotic treatments and have been remarkably successful in several applications. Their applicability may, however, be restricted due to the assumptions that need to be made for the media (see, e.g., [3, 4, 7]). Numerical (as contrasted to analytical) approaches to homogenization are typically based on building multiscale basis functions into the spatial discretization. Methods along this line of approach can be found in [16, 17, 18, 30, 32] and are the subject of active research.

*Received by the editors September 14, 2004; accepted for publication (in revised form) April 8, 2005; published electronically September 8, 2005. This work was partially supported through DARPA, AFOSR, and an NSF/ITR grant.
http://www.siam.org/journals/mms/4-3/61500.html
†Department of Chemical Engineering, Princeton University, Princeton, NJ 08544. Current address: Department of Mathematics, Purdue University, West Lafayette, IN 47907 (dxiu@math.purdue.edu).
‡Department of Chemical Engineering, Princeton University, Princeton, NJ 08544 (yannis@princeton.edu).

Alternatively, we can choose to model the medium properties as *random* fields, to account for our insufficient knowledge and/or measurement error. For example, field data indicate that the conductivity of many natural porous formations can be accurately described by a lognormal distribution (see, e.g., [9]). The homogenization techniques developed for *deterministic media* can be generalized to *random media*, and a comprehensive review can be found in [33].

In addition to deriving equations describing an effective medium, as homogenization does, many efforts have been devoted to direct detailed simulations of *random* media. In this context, the corresponding governing equations, e.g., the diffusion equation, Darcy's law, etc., are cast in the form of stochastic equations and solved as such directly. This approach further complicates the problem, since the governing equations are now defined in (much) higher-dimensional spaces, composed of both the physical space and the space accounting for the parameterization of the medium randomness (the random space). The most straightforward numerical approach is the Monte Carlo method (see, e.g., [8]), where repetitive deterministic simulations are conducted for particular realizations of the random functions describing the medium properties, and what we are interested in here is the *statistics* of the solution. This approach, based on random sampling, can be computationally expensive because the convergence rate of the ensemble averages, e.g., mean solution, is relatively low. (Monte Carlo simulations consisting of M realizations converge at a rate of $1/\sqrt{M}$.) There has been, therefore, a continuing interest in constructing nonsampling methods, which include perturbation methods [22], second-moment analysis [26], stochastic Galerkin methods [39, 2, 15], etc. Among them, the stochastic Galerkin methods, also called "generalized polynomial chaos" expansions, have been successful in many applications, when the basis functions in the random space are appropriately chosen. In particular, when the solution is sufficiently smooth in the random space, stochastic Galerkin methods converge exponentially fast [40, 39, 2].

However, for the problem we intend to study in this paper—random media with short correlation length—the stochastic Galerkin methods become inefficient. This is because the short correlation length will induce a higher-dimensional random space, and subsequently a larger number of equations to be solved—the so-called curse of dimensionality. We remark that such a difficulty exists for all the existing nonsampling methods. On the other hand, although Monte Carlo methods are (formally) immune from such a curse of dimensionality, their inherently slow convergence rate can hardly improve the overall efficiency.

In this paper, we propose an equation-free, multiscale method to simulate diffusion in a random media with small-scale structure (short correlation length). The equation-free methods were first introduced in [38] and are designed to resolve multiscale problems efficiently. Such methods solve the equations for the effective, coarse-grained behavior without obtaining them in closed form; the quantities required for these computations (residuals, action of Jacobians, time derivatives) are *estimated* by solving the microscopic/stochastic model with appropriately chosen initial conditions over short times (and, in certain cases, only parts of the spatial domain). The numerical results of these appropriately initialized short bursts of microscopic computations are used to estimate the rate of change (or other quantities of interest) of appropriately defined *observables*: macroscopic variables characterizing the coarse-grained evolution. These rates are then used by *projective integration* to evolve the coarse-grained observables in time with (hopefully much) larger time steps [11, 12, 34]. Thus, the time-consuming microscopic solvers are used for only a (small) fraction of the overall time integration, and no explicit knowledge of the equations governing the

macroscopic variables is required (equation-free). This framework has been applied to a variety of problems, ranging from bifurcation analysis of complex systems to homogenization of periodic media [11, 14, 21, 25, 28, 29, 35, 36].

For the random media with rough structure considered in this paper, we employ the Monte Carlo method as the "fine-scale" solver. An orthogonal polynomial expansion of the fine-scale solution is conducted (in principle) at every point in the physical space. Our coarse-grained observables are the first few expansion coefficients of such pointwise polynomial expansions on a relatively coarse grid; the key assumption underlying our method is that *in principle* it should be possible to write a closed equation for these observables that can successfully describe the (long term) evolution of the solution statistics.

The particular assumption (observation) in this paper is that, although each individual realization of the solution is characterized by small spatial scales, induced by the small scales in the diffusivity field, ensemble solution averages are characterized by larger, "coarser" scales. That is, after possibly a short initial transient (relaxation), the ensemble solution averages are significantly smoother than individual realizations in space and can therefore be accurately approximated with (hopefully significantly) fewer degrees of freedom (e.g., on a coarse mesh). This, in turn, implies that a closed equation exists (whether we can explicitly derive it or not) for these averages on a coarser mesh; this is precisely the equation that we will try to solve in this paper, without explicitly deriving it.

The coefficients of the pointwise polynomial expansion of the random solutions are representative of such ensemble averages and are observed to be smoother functions in space. We thus expect that they can indeed be represented on a coarse mesh. Since the explicit form of the governing equations for the evolution of such coefficients is unknown (to our best knowledge), we employ the equation-free framework to compute with it. In effect, we are trying to combine the simplicity of the Monte Carlo implementation with the strengths of (generalized) polynomial chaos representation: instead of deriving and discretizing the equations for the appropriate polynomial chaos coefficients via Galerkin expansion, we try to solve these equations through the design of "just enough" short computational experiments with the detailed direct solvers. To this end, the rate of change of these coarse-grained variables is estimated numerically from short bursts of fine-scale computation and propagated in time with larger steps via the projective integration technique. The advantage of the present definition of the coarse variables is that it allows us to reconstruct representative ensembles of fine-scale solutions with controlled accuracy. Numerical examples are presented to document the accuracy and efficiency of the new algorithm.

The paper is organized as follows. In section 2 we formulate the mathematical framework for diffusion in a random medium, and subsequently the multiscale problem we will study. In section 3 we present the details of the construction of our "equation-free" multiscale algorithm; in particular we focus on the "lifting" step: the construction of representative ensembles of fine-scale solution realizations. Numerical examples are presented in section 4, and we conclude the paper with a general discussion in section 5.

2. Unsteady diffusion equations in random media. In this section, we begin by presenting the mathematical framework for diffusion in a random medium. We then formulate the multiscale problem that we will study and discuss the difficulties in solving it efficiently.

2.1. Formulations for random diffusion. Let $D \in \mathbb{R}^d$, $d = 1, 2, 3$, be a bounded polygonal domain, let $J = (0, T] \in \mathbb{R}^+ = (0, \infty)$, for some fixed time $T > 0$, and let $(\Omega, \mathcal{F}, P)$ be a complete probability space. Here Ω is the set of outcomes, $\mathcal{F} \subset 2^\Omega$ is the σ-algebra of events, and $P : \mathcal{F} \to [0, 1]$ is a probability measure. Let $D_T = D \times J$, and we study the following random diffusion equation: find a stochastic function, $u : \Omega \times \bar{D}_T \to \mathbb{R}$, such that for P-almost everywhere $\omega \in \Omega$, the following equation holds:

$$\begin{cases} u_t(\omega, \cdot) - \nabla \cdot (\kappa(\omega, x)\nabla u(\omega, \cdot)) = f(\omega, \cdot) & \text{in } D_T, \\ u(\omega, \cdot) = 0 & \text{on } \partial D \times [0, T], \\ u(\omega, \cdot) = u_0(\omega, x) & \text{on } D \times \{t = 0\}, \end{cases} \tag{2.1}$$

where u is the unknown and $u_t = \partial u/\partial t$ its time derivative. $\kappa, u_0 : \Omega \times D \to \mathbb{R}$ and $f : \Omega \times D_T \to \mathbb{R}$ are known stochastic functions with continuous and bounded covariance functions. Denote by $B(A)$ the Borel σ-algebra generated by the open subsets of A; then κ and u_0 are assumed to be measurable with the σ-algebra $(\mathcal{F} \otimes B(D))$ and f with $(\mathcal{F} \otimes B(D_T))$.

The following assumptions are made on the input stochastic data:

1. κ is bounded and uniformly coercive, i.e.,

$$\exists\, \kappa_{\min}, \kappa_{\max} \in (0, +\infty) : P\left(\omega \in \Omega : \kappa(\omega, x) \in [\kappa_{\min}, \kappa_{\max}]\ \forall x \in \bar{D}\right) = 1. \tag{2.2}$$

   Also, κ has a uniformly bounded and continuous first derivative; i.e., there exists a real deterministic constant C such that

$$P\left(\omega \in \Omega : \kappa(\omega, \cdot) \in C^1(\bar{D}) \text{ and } \max_{\bar{D}} |\nabla_x \kappa(\omega, \cdot)| < C\right) = 1. \tag{2.3}$$

2. $f \in L^2(\Omega) \otimes L^2(D_T)$, i.e.,

$$\int_\Omega \int_J \int_D f^2(\omega, x, t) dx dt dP(\omega) < +\infty. \tag{2.4}$$

3. $u_0 \in L^2(\Omega) \otimes L^2(D)$, i.e.,

$$\int_\Omega \int_D u_0^2(\omega, x) dx dP(\omega) < +\infty. \tag{2.5}$$

2.2. Finite-dimensional noise and variational form. For the problem (2.1) to be practically solvable numerically, it should be possible to reduce the infinite-dimensional probability space to a finite-dimensional space. This can be accomplished by characterizing the probability space by a finite number of random variables. Such a procedure, termed as the "finite-dimensional noise assumption" in [2], is often achieved via a certain type of decomposition which can approximate the target random process with desired accuracy. One of the choices is the Karhunen–Loève-type expansion [27], which is based on the spectral decomposition of the covariance function of the input random process (see, e.g., [15, 39]). Following a decomposition and assuming that the random inputs can be characterized by N random variables, we can rewrite the random inputs in the abstract form

$$\kappa(\omega, x) = \kappa(Y_1(\omega), \ldots, Y_N(\omega), x) \text{ and } f(\omega, x, t) = f(Y_1(\omega), \ldots, Y_N(\omega), x, t), \tag{2.6}$$

where $N \geq 1$ is a finite integer and $\{Y_n\}_{n=1}^N$ are real random variables with zero mean value and unit variance and whose images $\Gamma_{n,N} \equiv Y_n(\Omega)$ are bounded intervals in $\mathbb{R}$ for $n = 1, \ldots, N$. Moreover, we assume that each Y_n has a density function $\rho_n : \Gamma_{n,N} \to \mathbb{R}^+$ for $n = 1, \ldots, N$, and we denote $\rho(y)$ for all $y \in \Gamma$ the joint probability density of $(Y_1, \ldots, Y_n)$ and $\Gamma \equiv \prod_{n=1}^N \Gamma_{n,N} \subset \mathbb{R}^N$ the support of such density. The expectation operator is subsequently defined as $\mathbb{E}(f) = \int_\Gamma f(y)\rho(y)dy$. Note that when random variables Y_n, $n = 1 \ldots, N$, are independent, we have $\rho(y) = \prod_{n=1}^N \rho_n(y_n)$ for all $y \in \Gamma$.

After the finite-dimensional characterization of the random inputs (2.6), the unsteady diffusion equation (2.1) can be expressed in the following strong form:

(2.7)
$$\begin{cases} u_t(y,x,t) - \nabla \cdot (\kappa(y,x)\nabla u(y,x,t)) = f(y,x,t) & \forall (y,x,t) \in \Gamma \times D \times J, \\ u(y,x,t) = 0 & \forall (y,x,t) \in \Gamma \times \partial D \times [0,T], \\ u(y,x,0) = u_0(y,x) & \forall (y,x) \in \Gamma \times D. \end{cases}$$

Often we seek its weak solution satisfying the following variational form: find $u \in L^2_\rho(\Gamma) \otimes L^2(0,T; H^1_0(D))$ with $u_t \in L^2_\rho(\Gamma) \otimes L^2(0,T; H^{-1}(D))$ such that

(2.8)
$$\begin{cases} \mathcal{I}_\rho(u_t, v) + \mathcal{K}_\rho(u, v; \kappa) = \mathcal{I}_\rho(f, v) & \forall v \in L^2_\rho(\Gamma) \otimes H^1_0(D), \\ u(t=0) = u_0, \end{cases}$$

where

$$\mathcal{I}_\rho(v,w) = \int_\Gamma \rho(y) \int_D v(y,x)w(y,x)dxdy$$

and

$$\mathcal{K}_\rho(v,w;\kappa) = \int_\Gamma \rho(y) \int_D \kappa(y,x)\nabla v(y,x) \cdot \nabla w(y,x)dxdy.$$

Note that problem (2.7) or (2.8) becomes an $(N+d)$-dimensional problem, where d is the dimensionality of the physical space D and N is the dimensionality of the random space Γ.

2.3. Formulations for multiscale problems. In this section we formulate the multiscale problem associated with the stochastic diffusion equation (2.1). In particular, we consider the problem where the random inputs, e.g., diffusivity κ, have very small correlation length $l_\kappa \ll 1$, compared to the (macroscopic) domain of interest D_T. For notational convenience, hereafter we restrict our exposition to problems with only κ being the random input and study, for P-almost everywhere $\omega \in \Omega$,

$$\frac{\partial u^\varepsilon}{\partial t}(\omega, \cdot) = \nabla \cdot \left[\kappa\left(\omega, \frac{x}{\varepsilon}\right) \nabla u^\varepsilon(\omega, \cdot)\right] + f(x) \qquad \text{in } D_T, \tag{2.9}$$

$$u^\varepsilon(\omega, \cdot) = 0 \qquad \text{on } \partial D \times [0,T], \tag{2.10}$$

$$u^\varepsilon(\omega, \cdot) = u_0^\varepsilon(x) \qquad \text{on } D \times \{t = 0\}. \tag{2.11}$$

Here we have assumed that the diffusivity κ satisfies the conditions (2.2) and (2.3) and is a homogeneous random field with a short correlation length $l_\kappa \sim O(\varepsilon) \ll O(1)$, i.e.,

$$C_\kappa(x,y) = C(|x-y|/l_\kappa) \qquad l_\kappa \sim O(\varepsilon) \ll O(1),\ (x,y) \in \bar{D} \times \bar{D}, \tag{2.12}$$

where $C_v(x,y) \equiv \mathbb{E}\left[(v(\omega,x)-\mathbb{E}[v(\omega,x)])(v(\omega,y)-\mathbb{E}[v(\omega,y)])\right]$ is the two-point covariance function and l_κ is the correlation length. Again we characterize the diffusivity field $\kappa(\omega, x/\varepsilon)$ by N independent random variables as in (2.6). Hence, problem (2.9) is in $(N+d)$ dimensions, and we can formulate it in the strong and weak forms similar to (2.7) and (2.8), respectively.

The discretization in the spatial domain $D \subset \mathbb{R}^d$ can be conducted via any standard technique, e.g., finite difference, finite elements, etc., with a maximum mesh spacing parameter $\delta > 0$. To fully resolve (2.9), we need to employ a fine mesh with $\delta < \varepsilon$. From a numerical point of view, very small mesh spacing δ often results in restrictions on the size of time steps of numerical schemes, and such restrictions are particularly severe for explicit schemes. Hence, a fine-scale computation of (2.9) requires computations with very small time steps on a very fine mesh.

The discretizations in the N-dimensional random space Γ can be conducted in different ways. The recently developed stochastic Galerkin methods, or generalized polynomial chaos, are extensions of the classical polynomial chaos which is based on the Wiener–Hermite expansion [15]. These extensions include the non-Hermite global orthogonal polynomial expansion from the Askey scheme [40, 39, 42], piecewise polynomial expansions [1, 2, 6], and wavelet basis [23, 24]. The stochastic Galerkin methods have fast convergence as the polynomial order is increased. In fact, under sufficient regularity requirements, exponential convergence has been proved for stochastic elliptic equations in [2] and shown numerically for various stochastic equations in [40, 39, 41]. The total number of expansion terms, K, however, depends not only on the order of polynomials but also on the dimensionality N of the random space. When $N \gg 1$ is very large, K increases fast with increasing order of polynomials. This significantly reduces the convergence rate with respect to the number of expansion terms for stochastic Galerkin methods. To this end, it may be necessary to resort to the Monte Carlo method, as its convergence rate, $1/\sqrt{M}$, where M is the number of realizations, albeit slower, is independent of the value of N.

The number of random variables, N, used to represent the random process $\kappa(\omega, x)$ depends on, among other factors, the correlation length of κ. Although one may choose different decomposition methods, in general, the value of N is inversely proportional to the correlation length l_κ. For the problem we consider here, $l_\kappa \ll O(1)$ implies $N \gg 1$, and problem (2.9) is in a high-dimensional random space. Subsequently, the fine-scale computation of (2.9) requires a large number of discretization terms in the N-dimensional random space Γ (by either a large number of expansion terms from a stochastic Galerkin method at a given order or a large number of realizations from a Monte Carlo method), a fine mesh in the physical space D to resolve the small scales induced by $l_\kappa \ll O(1)$, and very small time steps in the time domain J. Such computations can be prohibitively time consuming.

3. An equation-free multiscale method. In this section we present an equation-free multiscale method for the integration of (2.9); other tasks (such as fixed point algorithms for its stationary states) can also be formulated in an equation-free context (see the discussion in section 5). The key feature of the method is that the costly fine-scale computations of (2.9) are conducted only for a small fraction of the total

integration time. During the fine-scale computations, the rate of change of appropriate coarse-scale variables is estimated numerically, and subsequently represented on a coarser mesh and integrated in time with large time steps. The choice of such coarse variables is based upon the following assumption (observation): although each individual realization of the solution of (2.9) is characterized by small spatial scales, the ensemble averages, e.g., moments, of the solutions are significantly smoother in space (characterized by much larger scales), i.e.,

$$\mathbb{E}\left[g\left(u^{\varepsilon}\left(\omega, \frac{x}{\varepsilon}, t\right)\right)\right] = U_g(x,t) \qquad \forall g \in \mathcal{C}, \tag{3.1}$$

where $\mathcal{C}$ denotes a set of smooth functions. Variables $U_g(x,t)$ are the "coarse-grained" variables, and we will describe in detail their construction in the following section. Hereafter, we will drop the superscript ε of the fine-scale variables u^{ε}.

Equation (2.9) defines an evolutionary process,

$$\frac{\partial u}{\partial t}(\omega, x, t) = r(u), \qquad (\omega, x) \in \Omega \times D, \tag{3.2}$$

characterized by a solution operator $\{s(t)\}$, which forms a semigroup $u(\cdot, t) = s(t)u(\cdot, 0)$ in $t \in J$. We will assume that the set of properly defined coarse-scale variables from (3.1) satisfy, possibly after a short transient (relaxation) period, *closed* differential equations

$$\frac{\partial U_g}{\partial t}(x,t) = R(U_g), \qquad (x,t) \in D_T. \tag{3.3}$$

Note that typically one has several coarse variables. Subsequently, U_g is a vector field, and (3.3) is a system of equations. We also remark that the explicit knowledge of (3.3) may not be easy to obtain or may be too complicated to be of any practical use if it were known.

The general procedure for the equation-free projective integration methods (see, e.g., [11, 21, 20]) over one global time step Δt, starting at $t = t^n$ and ending at $t = t^{n+1}$, consists of the following key components:

- a "restriction" operator $\mathcal{P}$ to evaluate the coarse-grained variables from the ensemble of fine-scale computations, i.e., $U_g = \mathcal{P}u$, and a "lifting" operator $\mathcal{Q}$ to construct the representative ensemble of fine-scale solutions from the coarse-scale variables, i.e., $u = \mathcal{Q}U_g$;
- $n_f > 1$ steps of fine-scale computations of (3.2) with a small time step δt, where we will define $\Delta t_f = n_f \delta t$ and an intermediate time level $t_c^n = t^n + \Delta t_f$;
- one step of coarse projective integration of the coarse-scale equation (3.3) with a time step of the size $\Delta t_c = n_c \delta t, n_c > 1$.

Since Δt_c is associated with the time scale of the coarse variables U_g defined in (3.1), we usually have $n_c \gg 1$. The global time step is $\Delta t = t^{n+1} - t^n = \Delta t_f + \Delta t_c = (n_f + n_c)\delta t$. Figure 3.1 is a graphical illustration of the notation.

Specifically, for the multiscale diffusion problem in a random medium described by (2.9), the equation-free integration over one global time step Δt consists of the following steps (given a fine and coarse computational mesh and that $U_g^n(x) \equiv U_g(x, t^n)$ on the *coarse mesh*):

1. *Lifting* (or *reconstruction*): Generate an ensemble of random solutions $u^n(\omega, x) \equiv u(\omega, x, t^n)$ on the fine mesh.

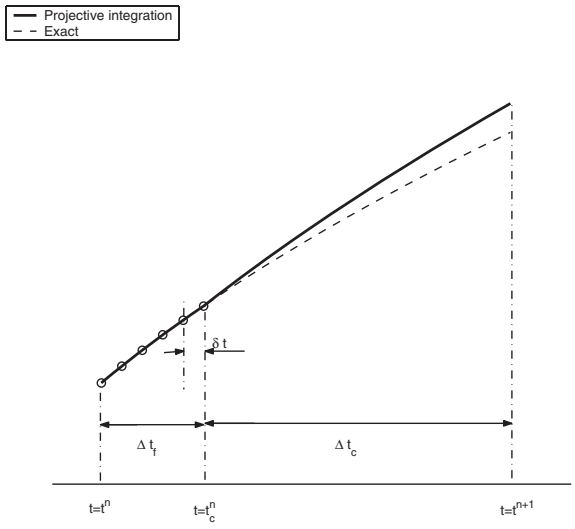

FIG. 3.1. *Sketch of the multiscale equation-free integration over one global time step.*

2. *Fine-scale computation*: Fully resolve (2.9) by using the fine mesh in D, a small time step δt in J, and an appropriate method in Γ (e.g., the Monte Carlo method). Such a fine-scale integration is conducted only for a short period of time, from t^n to the intermediate time t_c^n, i.e., $u(\cdot, t) = s(t)u(t^n)$, for $t^n \le t \le t_c^n = t^n + n_f \delta t$. Here $n_f \ge 1$ such that $n_f \delta t_f \sim t_R \ll t_M$, where t_R is the local relaxation time of the fine-scale process and is assumed to be much shorter than t_M, the typical time scales of the coarse-scale process (3.3).
3. *Restriction*: Evaluate the coarse variables $U_g(t)$ defined in (3.1) on the coarse mesh for $t^n \le t \le t_c^n$.
4. *Coarse-scale integration*: Estimate the time derivatives of the coarse variables U_g at $t = t_c^n$ and integrate the coarse-scale equations (3.3) to t^{n+1} via the projective integration method *on the coarse mesh*, with a time step $\Delta t_c = n_c \delta t = t^{n+1} - t_c^n$. Here $\Delta t_c \sim t_M \gg t_R$.

We now present a detailed description of each of the steps, starting with the more straightforward step—the fine-scale computation.

3.1. Fine-scale computation. The objective of the fine-scale computation is to fully resolve (2.9). To this end, any conventional spatial and temporal discretization scheme can be employed, e.g., finite difference or finite elements. Since the dimensionality is high ($(N + d)$-dimensional), we employ a Monte Carlo simulation (MCS) in the random space Γ. Here we illustrate the formulation of a Monte Carlo finite element method (MCFEM).

Denote $X_\delta^d \subset H_0^1(D)$, $D \subset \mathbb{R}^d$, a family of piecewise linear finite element approximation spaces, with a maximum mesh spacing parameter $\delta > 0$. This is the *fine mesh*, as we choose $\delta < O(\varepsilon) \ll O(1)$ to fully resolve all spatial scales. We shall assume all the standard assumptions on the finite element triangulation and its approximation estimate, i.e.,

$$\min_{\chi \in X_\delta^d} \|v - \chi\| \le C\delta \|v\|_{H^2(D)} \qquad \forall v \in H^2(D) \cap H_0^1(D), \tag{3.4}$$

where $C > 0$ is a constant independent of v and δ.

The MCFEM formulation for (2.9) is as follows:

- Prescribe the number of realizations, M, and a piecewise linear finite element space on D, X_δ^d, defined as above.
- For each $j = 1, \ldots, M$, sample independently and identically distributed realizations of the diffusivity $\kappa(\omega_j, \cdot)$ and find the corresponding approximation $u_\delta(\omega_j, \cdot) \in L^2(0, T; X_\delta^d)$ with $\frac{\partial u_\delta}{\partial t} \in L^2(0, T; (X_\delta^d)')$ such that

(3.5)
$$\left(\frac{\partial u_\delta}{\partial t}(\omega_j, \cdot), \chi\right)_\delta + \int_D \kappa(\omega_j, \cdot)\nabla u_\delta(\omega_j, \cdot) \cdot \nabla \chi dx = (f, \chi)_\delta \quad \forall \chi \in X_\delta^d,\ t \in J,$$

  where $(\cdot, \cdot)_\delta$ is the usual inner product in X_δ^d.
- Process the solution ensemble to generate statistics, e.g., $\mathbb{E}(u) = \frac{1}{M}\sum_{j=1}^M u_\delta(\omega_j, \cdot)$.

For more detailed discussion on the stochastic finite element spaces for elliptic problems, see [2]; for numerical examples and implementations of stochastic Galerkin methods for steady/unsteady diffusion equations, see [39, 42].

3.2. Restriction and lifting. The *restriction* from the fine-scale variables u to coarse-scale variables U_g consists of two steps: "random restriction" and "spatial restriction." First, the fine-scale variables u are averaged to U_g in the random space according to (3.1) (random restriction); then the coarse variables U_g are further restricted from the fine mesh to the coarse mesh (spatial restriction) justified by the assumption/observation that they are smoother. The *lifting procedure* is the reverse of the restriction. We now describe the details of the two procedures in both the random space Γ and the physical space D.

3.2.1. Operations in random space. The solution of the fine-scale computation via the MCFEM in section 3.1, or other effective methods, generates an ensemble of M realizations of the random solution u_δ at any $x \in X_\delta^d$ and $t \in J$. For any fixed (x, t), $u_\delta(\omega, \cdot)$ is a random variable, and we seek to represent such a random variable by an orthogonal polynomial approximation and define the expansion coefficients as our coarse-grained observables (variables). Hereafter we drop the subscript δ in u_δ, the fine-scale numerical solution of u, and seek to approximate it by $\mathcal{I}_\omega u$ for any fixed (x, t),

$$u(\omega, x, t) \simeq \mathcal{I}_\omega u(\omega, x, t) = \sum_{k=0}^K \bar{U}_k(x, t)\Phi_k(\xi(\omega)), \tag{3.6}$$

where $\{\Phi_k(\xi(\omega))\}_{k=0}^K$ is a set of orthogonal polynomials $\{\Phi\}$ in terms of random variable $\xi(\omega)$. The expansion coefficients are determined by

$$\begin{aligned} \bar{U}_k &= \frac{1}{\int_\Omega \Phi_k^2 dP}\int_\Omega u(\omega, \cdot)\Phi_k(\xi(\omega))dP(\omega) \\ &= \frac{1}{\mathbb{E}\left[\Phi_k^2\right]}\mathbb{E}\left[u(\omega, \cdot)\Phi_k(\xi(\omega))\right], \quad k = 0, \ldots, K, \end{aligned} \tag{3.7}$$

where the orthogonality of the basis functions has been used. Such a representation of random variables is commonly used in practice (cf. [15, 40, 39]). The correspondence between the type of orthogonal polynomials $\{\Phi\}$ and the type of random variable $\xi(\omega)$

includes Hermite–Gaussian, Jacobi-beta, Laguerre-gamma, etc. (see [40] for details). The convergence of such orthogonal polynomial expansions is assumed to be of the form

$$\|u(\omega,\cdot)-\mathcal{I}_\omega u(\omega,\cdot)\|_{L^2(\Omega)}=O(K^{-\gamma_\omega})\to 0,\qquad K\to\infty,\ \gamma_\omega>0, \tag{3.8}$$

where we have assumed the convergence rate scales as $K^{-\gamma_\omega}$ for some positive number $\gamma_\omega > 0$, which depends on the smoothness of $u(\omega)$. We remark that a complete theoretical analysis on the convergence of different bases remains an open issue. For numerical examples of the approximations of a random variable via different sets of bases, see [40].

The expansion coefficients $\{\bar{U}\}_{k=1}^K$ are the ensemble averages of u, as defined in (3.7), and under assumption (3.1), they become the coarse variables with larger spatial scale, i.e., with smoother profiles in the physical space D. For instance, the coefficient $\bar{U}_0(x,t)$ is the mean field of u and is in general smooth.

The finite-term polynomial approximation (3.6) defines two operations between u and $\{\bar{U}_k\}$, i.e., the "restriction" operator in random space $\mathcal{P}_\omega$ such that

$$\{\bar{U}_k(\cdot)\}_{k=0}^K=\mathcal{P}_\omega u(\omega,\cdot) \tag{3.9}$$

and the "lifting" operator $\mathcal{Q}_\omega$ such that

$$\mathcal{I}_\omega u(\omega,\cdot)=\mathcal{Q}_\omega\{\bar{U}_k(\cdot)\}_{k=0}^K, \tag{3.10}$$

where operation $\mathcal{P}_\omega$ is accomplished by (3.7) and $\mathcal{Q}_\omega$ by generating random samples of $\xi(\omega)$ in (3.6). Obviously both $\mathcal{P}_\omega$ and $\mathcal{Q}_\omega$ are linear operators, $\mathcal{Q}_\omega\mathcal{P}_\omega=\mathcal{I}_\omega$ and $\mathcal{I}_\omega\mathcal{I}_\omega=\mathcal{I}_\omega$.

We remark that the expansion (3.6) is different from the traditional polynomial chaos expansion. Expansion (3.6) is a pointwise approximation at fixed locations in (x,t), and hence requires only a one-dimensional (in the random space) polynomial basis of $\{\Phi_k(\xi(\omega))\}$, where the random variable $\xi(\omega)$ associated with the basis is different at different locations in the physical space. On the other hand, the traditional polynomial chaos expansion is written in the full N-dimensional random space for *all* locations of (x,t). While operators (3.9) and (3.10) are one-dimensional in the random space, they do not offer us an easy way to obtain the governing equations for the coarse variables $\bar{U}$, as shown in (3.3). (On the other hand, we can readily derive the governing equations in the N-dimensional random space via a Galerkin method if the traditional polynomial chaos expansion is employed.) We will show in the next section that we can circumvent the difficulty of not having the governing equations by using the "equation-free" approach.

3.2.2. Operations in physical space. Since we have assumed the coarse variables $\{\bar{U}_k(x,t)\}$ are smooth in space, they can be accurately represented on a coarse mesh $X_\Delta^d\subset D$, whose maximum mesh spacing $\Delta\gg\delta$. Such a representation can be expressed as, e.g., in terms of polynomial approximations in the physical space D,

$$\bar{U}_k(x,t)\simeq\mathcal{I}_x\bar{U}_k(x,t)=\sum_{l=1}^L\hat{\bar{U}}_{k,l}(t)\phi_k(x), \tag{3.11}$$

where $\{\phi_l(x)\}_{l=1}^L$ are the basis functions in X_Δ^d, and the expansion coefficients are defined as $\hat{\bar{U}}_{k,l}=(\bar{U}_k,\phi_l)_\Delta/(\phi_l,\phi_l)_\Delta$ for all k. Here $(\cdot,\cdot)_\Delta$ is the usual inner product

in X_Δ^d, and we have assumed, for notational convenience, that the bases are orthogonal. The completeness of such bases yields

$$\|\bar{U}_k(x,\cdot) - \mathcal{I}_x\bar{U}_k(x,\cdot)\|_{X_\Delta^d} = O(L^{-\gamma_{x,k}}) \to 0, \qquad L \to \infty,\ \gamma_{x,k} > 0\ \forall k, \tag{3.12}$$

where $\|\cdot\|_{X_\Delta^d}$ is an appropriate norm in X_Δ^d and $\gamma_{x,k} > 0$ quantifies the convergence rate, which depends on the smoothness of the underlying function $\bar{U}_k$.

Similarly, we can define two operators between $\bar{U}$ and $\{\hat{\bar{U}}_l\}$, i.e., the *restriction operator* $\mathcal{P}_x$ in the physical space D such that

$$\{\hat{\bar{U}}_{k,l}(\cdot)\} = \mathcal{P}_x\{\bar{U}_k(x,\cdot)\}, \qquad k = 0,\dots,K \text{ and } l = 1,\dots,L, \tag{3.13}$$

and the *lifting operator* $\mathcal{Q}_x$ such that

$$\mathcal{I}_x\{\bar{U}_k(x,\cdot)\} = \mathcal{Q}_x\{\hat{\bar{U}}_{k,l}(\cdot)\}, \qquad k = 0,\dots,K \text{ and } l = 1,\dots,L. \tag{3.14}$$

Clearly, we have $\mathcal{Q}_x\mathcal{P}_x = \mathcal{I}_x$ and $\mathcal{I}_x\mathcal{I}_x = \mathcal{I}_x$.

3.2.3. Global restriction and lifting. The global *restriction operator* $\mathcal{P}$ and *lifting operator* $\mathcal{Q}$ are thus defined as

$$\mathcal{P} = \mathcal{P}_x\mathcal{P}_\omega \text{ such that } \{\hat{\bar{U}}_{k,l}(t)\} = \mathcal{P}u(\omega,x,t) \tag{3.15}$$

and

$$\mathcal{Q} = \mathcal{Q}_\omega\mathcal{Q}_x \text{ such that } \mathcal{I}u(\omega,x,t) = \mathcal{Q}\{\hat{\bar{U}}_{k,l}(t)\}, \tag{3.16}$$

where the *global approximation operator* $\mathcal{I}$ is defined as

$$\mathcal{I} = \mathcal{Q}\mathcal{P} = \mathcal{Q}_\omega\mathcal{Q}_x\mathcal{P}_x\mathcal{P}_\omega = \mathcal{Q}_\omega\mathcal{I}_x\mathcal{P}_\omega. \tag{3.17}$$

Note the above operators are defined for $\omega = \{\omega_j\}_{j=1}^M \in \Omega$, $k = \{0,\dots,K\}$, $l = \{1,\dots,L\}$. A remarkable property of the operator $\mathcal{I}$ is that

$$\|u - \mathcal{I}u\| \to 0, \qquad K, L \to \infty, \tag{3.18}$$

where the norm $\|\cdot\|$ is defined in the tensor product space of $L^2(\Omega)$ and the appropriate space of D that defines the norm in (3.12). Such a property ensures that, by restricting from the fine-scale solution ensemble to the coarse-scale variables (operator $\mathcal{P}$) and lifting back to the fine-scale (operator $\mathcal{Q}$), we can reconstruct a representative ensemble of fine-scale solutions with controllable accuracy.

3.2.4. Implementation of restriction and lifting. In numerical simulations, the ensemble of solutions obtained by the Monte Carlo method in section 3.1, $\{u(\cdot,\omega_j)\}_{j=1}^M$, is first restricted in random space by $\mathcal{P}_\omega$ (3.9); the resulting variables $\{\bar{U}_k(x)\}$ on the fine mesh are further restricted to the coarse mesh by $\mathcal{P}_x$ (3.13).

The random restriction $\mathcal{P}_\omega$ is accomplished by (3.7), where the integral is written in a formal way as u and ξ in the integrand do not in general have the same probability measure. To integrate (3.7), we transform both the random variables u and ξ to a uniform variable $\theta \in U(0,1)$ via their cumulative density function (CDF), i.e., $\theta = F(u) = G(\xi)$, where F and G are the CDF of u and ξ, respectively. Hence,

$$u = F^{-1}(\theta), \qquad \xi = G^{-1}(\theta), \tag{3.19}$$

and (3.7) can be written as

(3.20)
$$\bar{U}_k = \frac{1}{\int_\Omega \Phi_k^2 dP}\int_\Omega u(\omega,\cdot)\Phi_k(\xi(\omega))dP(\omega) = \frac{1}{\int_\Omega \Phi_k^2 dP}\int_0^1 F^{-1}(\theta)\Phi_k(G^{-1}(\theta))d\theta.$$

The resulting integral in the bounded domain $(0,1)$ can be readily integrated using quadrature rules with sufficient accuracy. For more details on such integrations and numerical examples, see [40].

During the lifting procedure (3.16), the coarse variables on the coarse mesh are first "lifted" to the fine mesh via $\mathcal{Q}_x$ (3.14) (effectively, interpolated); the random lifting operation $\mathcal{Q}_\omega$ is then conducted to generate an ensemble of fine-scale solutions on the fine mesh. The spatial lifting $\mathcal{Q}_x$ is accomplished through (3.11) and the random lifting $\mathcal{Q}_\omega$ by (3.6). In (3.6), an ensemble of realizations of the random variable $\{\xi(\omega_j)\}_{j=1}^M$ are generated to, in turn, generate $\{u(\omega_j)\}_{j=1}^M$. The $\{\xi(\omega_j)\}_{j=1}^M$ is generated via (3.19) by using the same set of uniform random variable $\{\theta(\omega_j)\}_{j=1}^M$ resulted from the CDF of $\{u(\omega_j)\}_{j=1}^M$, i.e., $\theta = F(u)$. By using the same set of θ, the lifted solution $\{\mathcal{I}u(\omega_j)\}_{j=1}^M$ will have the same correlation structure as $\{u(\omega_j)\}_{j=1}^M$. This is a key step for efficient numerical computations, as it prescribes the "right" correlations between a particular realization of the medium and the corresponding solution for this medium.

3.3. Coarse-scale integration. As pointed out in section 3.2.1, although the pointwise expansion (3.6) utilizes only one-dimensional expansions in random space at fixed locations in physical space, it is unclear, to the authors' best knowledge, how the governing equations for the coarse variables $\{\hat{\bar{U}}_{k,l}\}$ should be; i.e., the right-hand side (RHS) of

$$\frac{\partial \hat{\bar{U}}_{k,l}}{\partial t} = R_{k,l}(\hat{\bar{U}}) \qquad \forall\ k \in [0,K],\ l \in [1,L] \tag{3.21}$$

is unknown. To circumvent the difficulty, we employ the "equation-free" approach where explicit knowledge of these governing equations is not needed. This procedure is as follows:

- Evaluate the coarse variables $\{\hat{\bar{U}}_{k,l}(t)\} = \mathcal{P}u(\cdot,t)$ from the fine-scale computation for $t^n \le t \le t_c^n = t^n + n_f\delta t$.
- Approximate the RHS of (3.21) at $t = t_c^n$, i.e.,

  (3.22)
  $$R_{k,l}(t_c^n) = \sum_{j=0}^{n_e}\alpha_j \hat{\bar{U}}_{k,l}(t_j) = \frac{d\hat{\bar{U}}_{k,l}}{dt}(t_c^n) + O(\delta t^{J_f}), \qquad k \in [0,K],\ l \in [1,L],$$

  where $1 \le n_e \le n_f$, $t_j = t_c^n - j\delta t$, and J_f denotes the order of the approximation. $\{\alpha_j\}_{j=1}^{n_e}$ is a set of consistent coefficients such that $\sum \alpha_j v(t_j) = dv/dt(t_c^n) + O(\delta t^{J_f})$.
- Once the RHS of (3.21) is estimated numerically, (3.21) is integrated forward in time for one step on a larger time step. For example, given coarse time step of size $\Delta t_c = n_c \cdot \delta t$ with $n_c \ge 1$, such that $t^{n+1} = t^n + \Delta t_c = t^n + (n_f + n_c)\delta t$, the Euler forward integrator takes the form

  $$\hat{\bar{U}}_{k,l}^{n+1} = \hat{\bar{U}}_{k,l}(t_c^n) + \Delta t_c \cdot R_{k,l}(t_c^n) + O(\Delta t_c^2), \qquad k \in [0,K],\ l \in [1,L]. \tag{3.23}$$

The estimation of derivatives (3.22) may suffer from numerical oscillations, especially for systems that exhibit noisy behavior at microscopic scales, e.g., molecular dynamics. In this case, certain smoothing techniques such as a least-square fit may be used to alleviate the problem [14]. (Such is not the case in this paper.) The integration of coarse variables (3.23) is a simple Euler forward scheme, which can lead to relatively large errors when Δt_c is large. Other integration schemes, such as higher-order single step methods or multistep methods, can be used for their improved accuracy and/or better stability properties [11, 12]. A complete analysis (stability, accuracy, etc.) of the equation-free method to stochastic equations is still lacking and is beyond the scope of the current paper. For an error analysis of the equation-free method for a deterministic system (flow simulation), see [37].

3.4. Computational complexity. Let us denote by $N_f \sim O(\delta^{-d})$ the number of degrees of freedom (DOF) of the fine mesh X_δ^d and by $N_c \sim O(\Delta^{-d})$ the DOF of the coarse mesh X_Δ^d. During the coarse integration step, the fine-scale computation by M realizations of MCSs is effectively reduced to a problem of the evolution of $(K+1)$ local polynomial expansion coefficients (3.6) on the coarse mesh obtained by the global restriction operator $\mathcal{P} = \mathcal{P}_x \mathcal{P}_\omega$. The reduction in computational complexity can be illustrated as

$$\mathbb{R}^{M\times N_f} \xrightarrow{\mathcal{P}_\omega} \mathbb{R}^{(K+1)\times N_f} \xrightarrow{\mathcal{P}_x} \mathbb{R}^{(K+1)\times N_c}. \tag{3.24}$$

Thus, to march problem (2.9) over a global time step $\Delta t = (n_f + n_c)\delta t$, the particular equation-free projective integration algorithm, which consists of n_f steps of fine-scale computations and one step of coarse integration, needs to solve a problem of complexity

$$C_c \sim n_f \times \mathbb{R}^{M\times N_f} + \mathbb{R}^{(K+1)\times N_c}. \tag{3.25}$$

On the other hand, the complexity of the full-scale MCFEM over the same time interval Δt is

$$C_f \sim (n_f + n_c) \times \mathbb{R}^{M\times N_f}. \tag{3.26}$$

For the multiscale problem considered in this paper, we have $N_f \gg N_c$, $O(1) \sim K \ll M$, and $n_c \gg n_f$. Thus, roughly speaking, $C_f/C_c \sim (1+n_c/n_f) \gg 1$. We remark that such an estimate is rather crude, and the actual computational efficiency is problem dependent.

4. Numerical results. In this section we present numerical results on (2.9) in one spatial dimension $x \in [0,1]$. The restriction and lifting operations in physical spaces, as shown in section 3.2.2, come from standard approximation theory, and here we focus on the properties of the *random restriction* and the *random lifting*. We remark that the method extends trivially to multidimensional physical spaces. We assume that $\kappa(\omega, x)$ is a Gaussian random field with unit mean value, i.e., $\mathbb{E}u(\omega, x) = 1$, and employ the Hermite polynomials in random space to represent the random field in (3.6). We employ the Gaussian random field model because of its ease of numerical generation. (Generation of non-Gaussian random fields is still an active research area.) From a mathematical point of view, Gaussian models are inappropriate for the diffusivity fields, as they allow negative values with nonzero probability, and thus violate the uniform coercivity assumption (2.2). In practice, however, such negative values are rare, especially when the variance is small, and we can neglect such negative

values if they occur in the random realizations. (In the numerical examples below, negative values never appear.)

We assume that the Gaussian random field has an exponential covariance function, i.e., $C_\kappa(x,y) = \exp(|x-y|)/l_\kappa$. Such a correlation function can be generated from a first-order Markov process and has been used extensively in the literature. All MCFEM computations are conducted by a linear finite element method with Euler forward integration, and $M = 1{,}000$ realizations are used. The forcing term in (2.9) is fixed at $f(x) \equiv -2$, and zero Dirichlet boundary conditions are imposed at $x = 0$ and $x = 1$. The restriction in physical space (3.11) is conducted on a set of Jacobi polynomial basis (see [19, Chapter 2]).

4.1. Accuracy. The complete error analysis of the present multiscale method remains an open issue. In this section, we conduct numerical experiments to document the error convergence. In the first example, we set $l_\kappa = 0.1$ and use 40 linear elements ($\delta = 0.025$). Fifth-order Hermite expansion ($K = 5$) is used for the random restriction (3.6) and fifth-order Jacobi basis ($L = 5$) for the spatial restriction (3.11). The time step for the fine-scale computation is $\delta t = 0.001$, and it is conducted for $n_f = 20$ steps. The coarse integration has a time step $\Delta t_c = 0.08$ (i.e., $n_c = 80$), so that the global time step is $\Delta t = (n_f + n_c)\Delta t_f = 0.1$. For this illustrative example, the computational speed-up is modest ($4 \sim 5$ times), because the separation of scales is modest.

Figure 4.1 shows the stochastic solution profile (mean and standard deviation) at time $T = 1$. Good agreements are obtained between the full-scale MCS and the equation-free multiscale method.

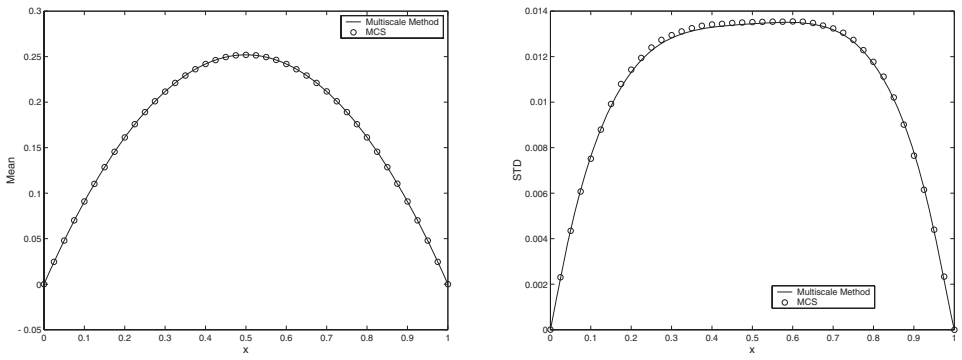

FIG. 4.1. *Solution profile at $T = 1$. Left: mean solution. Right: standard deviation.*

To study the error contributions from different factors, we conducted a series of computations with varying parameters. In Figure 4.2 the L^∞ errors in mean and standard deviation (STD) are shown. These computations have fixed values of $\Delta t_f = 0.05$, $K = 3$, and $L = 4$ and varying time steps Δt_c of the coarse integration. We observe that the errors decrease as the size of time steps for the coarse integration decreases.

To examine the error convergence with respect to the orders of approximation in random space (parameter K) and physical space (parameter L), we fix the time steps of integrations $\Delta t_f = \Delta t_c = 0.05$. The size of coarse integration Δt_c is sufficiently small such that the temporal errors are subdominant (e.g., $O(10^{-6})$ for the mean as shown from Figure 4.2). In Figure 4.3, the errors with increasing order of the

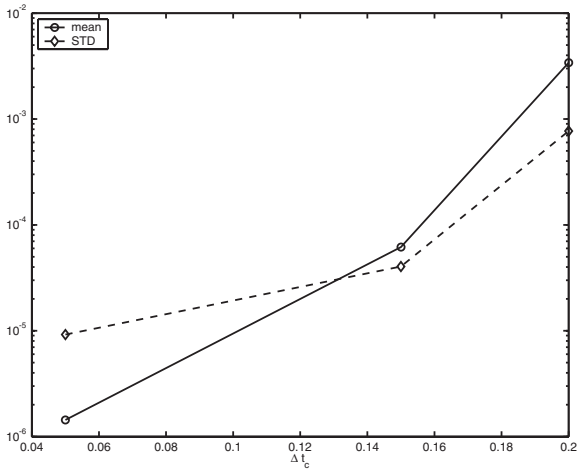

FIG. 4.2. *Errors in mean and STD versus the step size of the coarse integration.*

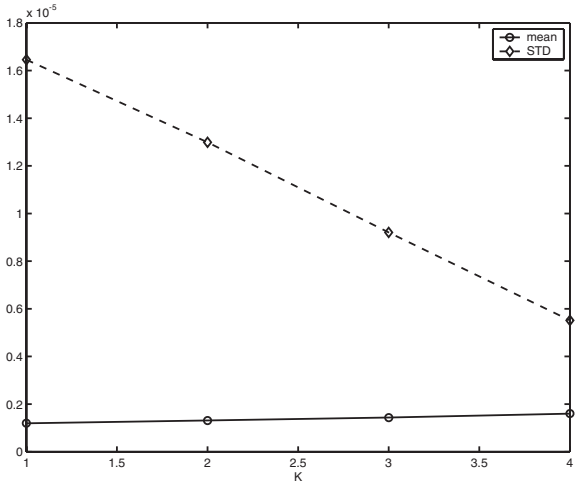

FIG. 4.3. *Errors in mean and STD versus the order of Hermite approximation of the coarse variables.*

Hermite approximations (K) in the random restriction $\mathcal{P}_\omega$ are shown. Fourth-order ($L = 4$) Jacobi basis is used in the physical space, so that the errors from spatial restriction $\mathcal{P}_x$ are subdominant. It can be seen that as the order K of the random restriction increases, the errors in STD decrease as expected. The mean solution is well resolved by even the first-order Hermite expansion ($K = 1$), and its errors remain at the $O(10^{-6})$ level.

We then fix the order of the Hermite approximation in the random space at third order, i.e., $K = 3$, and vary L. Again, $\Delta t_c = \Delta t_f = 0.05$ is sufficiently small. In Figure 4.4, it can be seen that the error in the mean solution quickly reaches a saturation level of $O(10^{-6})$ at second order $L = 2$. This is consistent with the result in Figure 4.3. The error in STD keeps decreasing with increasing order of L.

As discussed in section 3.2.3, the current implementations of the restriction operator $\mathcal{P}$ and the lifting operator $\mathcal{Q}$ allow us to reconstruct representative ensembles

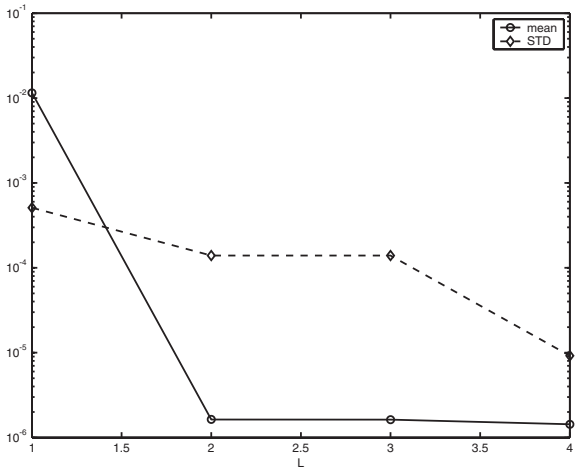

FIG. 4.4. *Errors in mean and STD versus the order of spatial representation of the coarse variables.*

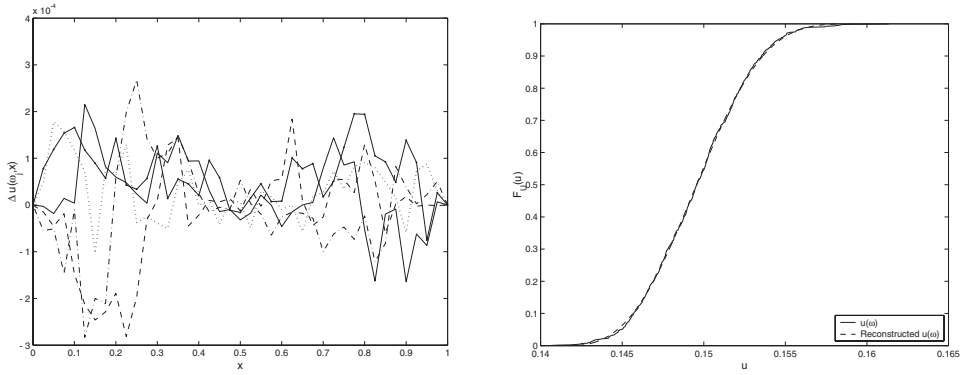

FIG. 4.5. *Comparison of random solution (u) and its lifting ($\mathcal{I}u$) at $t = 0.1$. Left: profiles of $u(\omega_j, x) - \mathcal{I}u(\omega_j, x)$ for some realizations of ω_j. Right: CDFs of u and $\mathcal{I}u$ at $x = 0.5$.*

of fine-scale solutions by restricting them to the coarse scale first and then lifting back to the fine scale; i.e., $\mathcal{I} = \mathcal{Q}\mathcal{P}$ is an approximation operator. To examine the properties of the global approximation operator $\mathcal{I}$ (3.17), we plot $\Delta u(\omega, x, t) = u(\omega, x, t) - \mathcal{I}u(\omega, x, t)$ at an arbitrary chosen time $t = 0.1$. On the left of Figure 4.5, several realizations of such errors (randomly chosen from the $M = 1{,}000$ realizations) are shown. It can be seen that the errors are bounded within a small range of the same order of the spatial error ($O(10^{-3})$). The CDF of the random solution u at the center of the domain ($x = 0.5$) is shown on the right of Figure 4.5. Again we see excellent agreement between the probability distribution of the target u and that of its lifting, $\mathcal{I}u$.

To further examine the error of $\mathcal{I}$, we plot on the left of Figure 4.6 the pointwise error of $\Delta u(\omega, x, t)$ at $x = 0.5$, $t = 0.1$ for all realizations ω_j, $j \in [1, 1{,}000]$. We observe that, except at a few discrete points, which belong to a set with *arguably* zero measure, the errors are bounded in a very small interval of order $O(10^{-3})$. On the right of Figure 4.6, we plot the pathwise correspondence of $u(\omega_j)$ versus $\mathcal{I}u(\omega_j)$ for

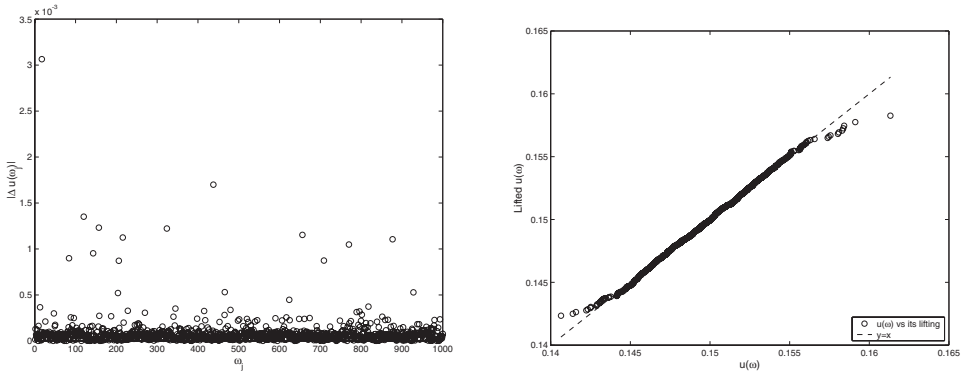

FIG. 4.6. *Comparison of random solution (u) and its lifting ($\mathcal{I}u$) at $t = 0.1$, $x = 0.5$. Left: pointwise error of $|u(\omega_j) - \mathcal{I}u(\omega_j)|$ for all ω_j, $j = 1, \ldots, 1{,}000$. Right: $\mathcal{I}u(\omega_j)$ versus $u(\omega_j)$.*

all $j = 1, \ldots, 1{,}000$. It is seen that the data collapse on $y = x$ where the exact correspondence should be. These results confirm that our $\mathcal{I}$ is indeed an approximation operator which allows us to reconstruct the fine-scale solution ensemble *with built in desired correlation structures* from the computed coarse solutions. To achieve this, it is important that one uses, during the lifting step (3.6), the same uniform random variable values determined by the numerical solutions at the restriction stage as described in section 3.2.4. If, however, a random variable ξ is used without maintaining the correct correlation structure between the medium realization and the solution in this medium, the lifted solutions will not be properly correlated to the true solutions, even if the ensemble is constructed to maintain the same distribution. Figure 4.7 shows such an example. Again, this is the numerical solution at $t = 0.1$, and we plot the realizations at $x = 0.5$. Here the numerical solutions are lifted by using arbitrarily generated Gaussian random variables ξ in (3.6). We observe that although the solution has the same distribution as the MCS solutions (Figure 4.7, left), it is completely uncorrelated to the true solution as shown on the right of Figure 4.7. The ability to maintain good correlation structure in the lifting procedure is a distinctive feature of our method. This is different from the conventional lifting procedures, whose reconstructed solutions are rather arbitrary (to a certain degree), and a certain constraining procedure or a relaxation integration is needed to "heal" the lifted solution ensemble [13, 10].

4.2. Efficiency. In the second example, we prescribe a diffusivity field with relatively small correlation length $l_\kappa = 0.01$. We employ 1,000 linear elements to resolve the small spatial scales ($\delta = 0.001$), and this results in a time scale of $O(10^{-6})$. Thus, we set the time step of the fine-scale computation at $\delta t = 10^{-6}$. The number of fine-scale computations within each global time step is $n_f = 1{,}000$, and the time step of the coarse integration is chosen as $\Delta t_c = n_c \delta t$ with $n_c = 49{,}000$. Thus, the global time step is $\Delta t = (n_f + n_c)\delta t = 0.05$. The polynomial orders are set at $K = 5$ and $L = 5$ for the restrictions in the random space and the physical space, respectively. For this application, we achieve computational speed-up of ~ 50, compared to the full-scale MCS. The random solution profiles in Figure 4.8 show again good agreement between the full-scale MCFEM and the multiscale computation. We remark that the quantification of the computational speed-up is problem dependent. In the diffusion problems considered here, such speed-up is smaller at the beginning

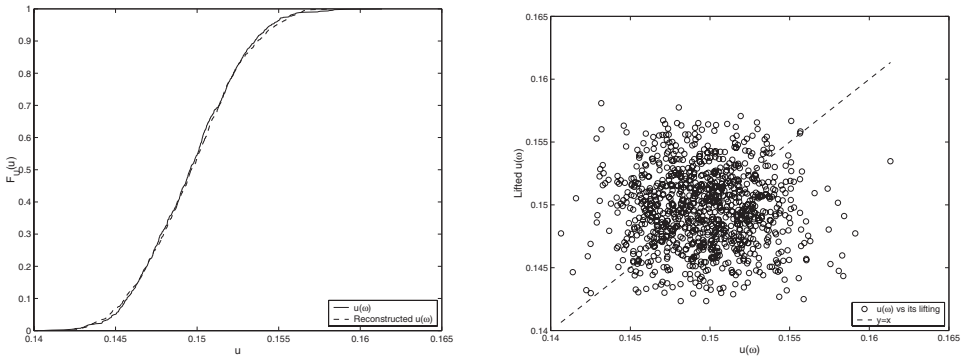

FIG. 4.7. *Comparison of random solution (u) and its lifting ($\mathcal{I}u$) without correct correlation structure at $t = 0.1$, $x = 0.5$. Left: CDF of u and $\mathcal{I}u$. Right: $\mathcal{I}u(\omega_j)$ versus $u(\omega_j)$ for $j = 1, \ldots, 1{,}000$.*

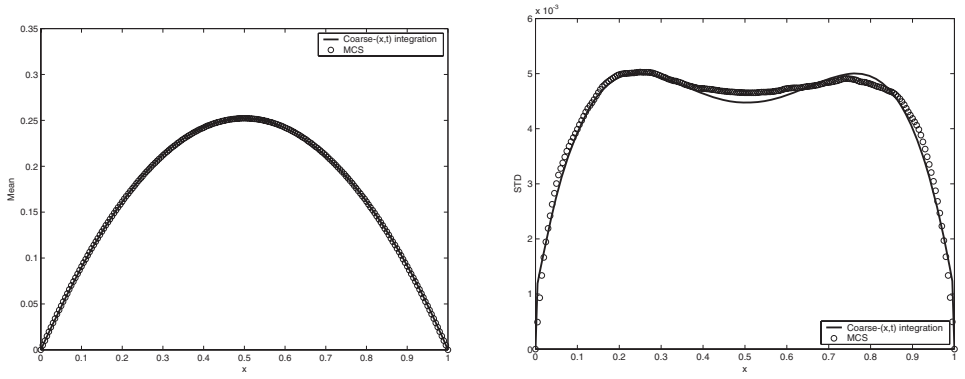

FIG. 4.8. *Solution profile at $T = 1$. Left: mean solution. Right: STD.*

of the computation due to the fast evolution of the solution. However, the speed-up is significantly larger once the initial transient is passed.

5. Summary. In this paper we present an equation-free multiscale algorithm for integrating unsteady diffusion problems in a random medium with small-scale spatial structures, e.g., short correlation length. The method is based on the assumption that although the individual realizations of the random solutions are characterized by small scales, their ensemble averages are much smoother, characterized by larger scales. This motivates the use of a set of coarse-grained observation variables, which are based on the pointwise polynomial approximations of the fine-scale random solutions. Such coarse-grained variables are approximated accurately on a coarse mesh and integrated in time with large time steps. An equation-free approach is employed for the coarse integration, as the explicit knowledge of the governing equations of the coarse variables is unavailable in closed form. Details of the multiscale method are presented, and its accuracy and efficiency are documented by numerical examples. In particular, we demonstrate that the present constructions of the restriction and lifting operators allow us to successfully reconstruct representative fine-scale solutions based only on the knowledge of the coarse solutions. Future work will include a complete analysis of error estimates of the current method and applications to more complicated systems.

It is interesting that, in this approach, one creates a "wrapper" around an existing direct detailed solver, using it as a black box; traditional stochastic Galerkin algorithms would require the writing of new code to solve the coupled system of equations in both physical and random space. Our approach can thus be considered as a "nonintrusive" one—the solution in both physical and random space is solved using an existing legacy code through a wrapper and sidestepping the effort of new code development and validation. In this paper the only numerical task we demonstrated in the equation-free context was *temporal integration*. Other tasks enabled through matrix-free iterative linear algebra (e.g., Newton–Krylov GMRES based fixed point solvers, Arnoldi-type eigensolvers) naturally fit in the equation-free framework; and many more can be performed on the explicitly unavailable coarse-grained equation: steady state and bifurcation computations, stability computations, equation-free optimization, and even dynamic renormalization. Finally, the smoothness *in space* of the coarse-grained variables can be exploited (via the so-called gap-tooth and patch dynamics equation-free schemes) to perform the fully resolved fine-scale computations not only for short times but also for only parts of the physical domain of interest [21, 36, 14]. Finally, although in this paper we have designed direct numerical experiments to *solve* the coarse-grained equation which is hypothesized to exist and close, it is worth noting that it is also possible to design direct numerical experiments to *test this hypothesis* (see [25]). These tasks, and the conditions under which they can be successfully performed in an equation-free framework and accelerate random computations, is the subject of ongoing research.

Acknowledgments. We would like to thank Dr. Ivo Babuška and Dr. Raul Tempone of ICES of the University of Texas, Austin, for useful discussions.

REFERENCES

[1] I. Babuška and P. Chatzipantelidis, *On solving elliptic stochastic partial differential equations*, Comput. Methods Appl. Mech. Engrg., 191 (2002), pp. 4093–4122.

[2] I. Babuška, R. Tempone, and G. E. Zouraris, *Galerkin finite element approximations of stochastic elliptic partial differential equations*, SIAM J. Numer. Anal., 42 (2004), pp. 800–825.

[3] G. P. A. Bensoussan and J.-L. Lions, *Asymptotic Analysis for Periodic Structures*, North–Holland, Amsterdam, 1978.

[4] D. Cioranescu and P. Donato, *An Introduction to Homogenization*, Oxford University Press, Oxford, UK, 1999.

[5] G. Dagan, *Flow and Transport in Porous Formations*, Springer-Verlag, Heidelberg, Berlin, New York, 1989.

[6] M. Deb, I. Babuška, and J. Oden, *Solution of stochastic partial differential equations using Galerkin finite element techniques*, Comput. Methods Appl. Mech. Engrg., 190 (2001), pp. 6359–6372.

[7] W. E, *Homogenization of linear and nonlinear transport equations*, Comm. Pure Appl. Math., 45 (1992), pp. 301–326.

[8] G. Fishman, *Monte Carlo: Concepts, Algorithms, and Applications*, Springer-Verlag, New York, 1996.

[9] R. Freeze, *A stochastic-conceptual analysis of one-dimensional groundwater flow in nonuniform homogeneous media*, Water Resour. Res., 11 (1975), pp. 725–741.

[10] C. W. Gear, T. J. Kaper, I. G. Kevrekidis, and A. Zagaris, *Projecting to a slow manifold: Singularly perturbed systems and legacy codes*, SIAM J. Appl. Dyn. Syst., 4 (2005), pp. 711–732.

[11] C. W. Gear and I. G. Kevrekidis, *Projective methods for stiff differential equations: Problems with gaps in their eigenvalue spectrum*, SIAM J. Sci. Comput., 24 (2003), pp. 1091–1106.

[12] C. Gear and I. Kevrekidis, *Telescopic projective methods for parabolic differential equations*, J. Comput. Phys., 187 (2003), pp. 95–109.

[13] C. Gear and I. Kevrekidis, *Constraint-defined manifolds: A legacy-code approach to low-dimensional computations*, J. Sci. Comput., submitted.
[14] C. Gear, J. Li, and I. Kevrekidis, *The gap-tooth method in particle simulations*, Phys. Lett. A, 316 (2003), pp. 190–195.
[15] R. Ghanem and P. Spanos, *Stochastic Finite Elements: A Spectral Approach*, Springer-Verlag, New York, 1991.
[16] T. Hou and X.-H. Wu, *A multiscale finite element method for elliptic problems in composite materials and porous media*, J. Comput. Phys., 134 (1997), pp. 169–189.
[17] T. Hou, X.-H. Wu, and Z. Cai, *Convergence of a multi-scale finite element method for elliptic problems with rapidly oscillating coefficients*, Math. Comp., 68 (1999), pp. 913–943.
[18] T. Hughes, G. R. Feijoo, L. Mazzei, and J.-B. Quincy, *The variational multiscale method – a paradigm for computational mechanics*, Comput. Methods Appl. Mech. Engrg., 166 (1998), pp. 3–24.
[19] G. Karniadakis and S. Sherwin, *Spectral/hp Element Methods for CFD*, Oxford University Press, New York, 1999.
[20] I. Kevrekidis, C. Gear, and G. Hummer, *Equation-free: The computer-assisted analysis of complex, multiscale systems*, AIChE J., 50 (2004), pp. 1346–1354.
[21] I. Kevrekidis, C. Gear, J. Hyman, P. Kevrekidis, O. Runborg, and C. Theodoropoulos, *Equation-free coarse-grained multiscale computation: Enabling microscopic simulators to perform system-level analysis*, Commun. Math. Sci., 1 (2003), pp. 715–762.
[22] M. Kleiber and T. Hien, *The Stochastic Finite Element Method*, John Wiley & Sons, Chichester, UK, 1992.
[23] O. Le Maitre, O. Knio, H. Najm, and R. Ghanem, *Uncertainty propagation using Wiener-Haar expansions*, J. Comput. Phys., 197 (2004), pp. 28–57.
[24] O. Le Maitre, H. Najm, R. Ghanem, and O. Knio, *Multi-resolution analysis of Wiener-type uncertainty propagation schemes*, J. Comput. Phys., 197 (2004), pp. 502–531.
[25] J. Li, P. G. Kevrekidis, C. W. Gear, and I. G. Kevrekidis, *Deciding the nature of the coarse equation through microscopic simulations: The baby-bathwater scheme*, Multiscale Model. Simul., 1 (2003), pp. 391–407.
[26] W. Liu, G. Besterfield, and A. Mani, *Probabilistic finite elements in nonlinear structural dynamics*, Comput. Methods Appl. Mech. Engrg., 56 (1986), pp. 61–81.
[27] M. Loève, *Probability Theory*, 4th ed., Springer-Verlag, New York, Heidelberg, 1977.
[28] A. Makeev, D. Maroudas, and I. Kevrekidis, *Coarse stability and bifurcation analysis using stochastic simulators: Kinetic Monte Carlo examples*, J. Chem. Phys., 116 (2002), pp. 10083–10091.
[29] A. Makeev, D. Maroudas, A. Panagiotopoulos, and I. Kevrekidis, *Coarse bifurcation analysis of kinetic Monte Carlo simulations: A lattice-gas model with lateral interactions*, J. Chem. Phys., 117 (2002), pp. 8229–8240.
[30] A. Matache, I. Babuška, and C. Schwab, *Generalized p-FEM in homogenization*, Numer. Math., 86 (2000), pp. 319–375.
[31] G. Milton, *Theory of Composites*, Cambridge University Press, Cambridge, UK, 2002.
[32] A. Oberai and P. Pinsky, *A multiscale finite element method for the Helmholtz equation*, Comput. Methods Appl. Mech. Engrg., 154 (1998), pp. 281–297.
[33] P. Renard and G. De Marsily, *Calculating equivalent permeability: A review*, Adv. Water Res., 20 (1997), pp. 253–278.
[34] R. Rico-Martinez, C. Gear, and I. Kevrekidis, *Coarse projective kMC integration: Forward/reverse initial and boundary value problems*, J. Comput. Phys., 196 (2004), pp. 474–489.
[35] O. Runborg, C. Theodoropoulos, and I. Kevrekidis, *Effective bifurcation analysis: A time-stepper based approach*, Nonlinearity, 15 (2002), pp. 491–511.
[36] G. Samaey, D. Roose, and I. G. Kevrekidis, *The gap-tooth scheme for homogenization problems*, Multiscale Model. Simul., 4 (2005), pp. 278–306.
[37] S. Sirisup, D. Xiu, G. Karniadakis, and I. Kevrekidis, *Equation-free/Galerkin-free POD-assisted computation of incompressible flows*, J. Comput. Phys., 207 (2005), pp. 568–587.
[38] C. Theodoropoulos, Y. Qian, and I. Kevrekidis, *Coarse stability and bifurcation analysis using time-steppers: A reaction-diffusion example*, Proc. Natl. Acad. Sci. USA, 97 (2000), pp. 9840–9843.
[39] D. Xiu and G. Karniadakis, *Modeling uncertainty in steady state diffusion problems via generalized polynomial chaos*, Comput. Methods Appl. Mech. Engrg., 191 (2002), pp. 4927–4948.
[40] D. Xiu and G. E. Karniadakis, *The Wiener–Askey polynomial chaos for stochastic differential equations*, SIAM J. Sci. Comput., 24 (2002), pp. 619–644.

[41] D. Xiu and G. Karniadakis, *Modeling uncertainty in flow simulations via generalized polynomial chaos*, J. Comput. Phys., 187 (2003), pp. 137–167.
[42] D. Xiu and G. Karniadakis, *A new stochastic approach to transient heat conduction modeling with uncertainty*, Inter. J. Heat Mass Trans., 46 (2003), pp. 4681–4693.